https://doi.org/10.3799/dqkx.2024.100

俯冲沉积物交代造山带岩石圈地幔：来自三江地区煌斑岩钾同位素的约束

刘嘉文[1,2]，田世洪[2*]，耿显雷[2]，梁正伟[2]，陈　露[2]

1. 东华理工大学地球科学学院，江西南昌　330013
2. 东华理工大学核资源与环境国家重点实验室，江西南昌　330013

摘　要：碰撞后富钾岩浆通常被认为是造山带岩石圈地幔中俯冲沉积物再循环的证据，钾同位素则是示踪再循环俯冲沉积物的良好指示剂.以三江地区煌斑岩为例，在主微量元素和常规同位素的基础上，开展了钾同位素研究，以探究三江地区岩石圈地幔源区特征.本研究发现剑川、北衙、盐源和姚安4个地区的煌斑岩样品均能代表地幔源区特征，与风化蚀变、分离结晶、地壳混染和动力学分馏过程无关，样品总体呈现较正常地幔偏轻的钾同位素特征((－0.61±0.02)‰～(－0.31±0.01)‰)，表明可能与俯冲沉积物交代有关，而与通常富集重钾同位素的流体无关.进一步通过蒙特卡洛模型端元混合模拟计算表明，4个地区表现出不同程度的俯冲沉积物混入，且姚安地区的沉积物比例可达到10%.这一结论进一步证实了钾同位素作为一种敏感的示踪剂，能够有效示踪地幔中再循环的俯冲沉积物组分.

关键词：钾；同位素；沉积物交代；三江地区；煌斑岩；造山带岩石圈地幔；地球化学.

中图分类号：P597　　**文章编号：**1000－2383(2024)11－3930－16　　**收稿日期：**2024－10－23

Subduction-Induced Sedimentary Metasomatism of Orogenic Lithospheric Mantle: Insights from Potassium Isotope in Lamprophyres of Sanjiang Region

Liu Jiawen[1,2], Tian Shihong[2*], Geng Xianlei[2], Liang Zhengwei[2], Chen Lu[2]

1. *School of Earth Sciences, East China University of Technology, Nanchang* 330013, *China*
2. *State Key Laboratory of Nuclear Resources and Environment, East China University of Technology, Nanchang* 330013, *China*

Abstract: Post-collisional potassic magmas are commonly regarded as evidence for the recycling of subducted sediments in the lithospheric mantle of orogenic belts, with potassium isotope serving as an excellent tracer for these recycled sediments. This study takes the lamprophyres from the Sanjiang region as an example, conducting potassium isotope analysis based on major and trace elements and Sr-Nd-Pb isotopes, to explore the characteristics of the lithospheric mantle source in the Sanjiang region. This study

基金项目：国家重点研发计划课题“北喜马拉雅锂等稀有金属找矿预测与勘查示范”(No. 2021YFC2901903)；江西省自然科学基金重点项目(No.20224ACB203011)；自然资源部深地科学与探测技术实验室开放课题(No.Sino Probe Lab 202217)；江西省“双千计划”创新领军人才长期项目(No.2020101003)；东华理工大学高层次人才引进配套经费(No.1410000874).

作者简介：刘嘉文(1996—)，女，博士生，主要从事同位素地球化学和矿床学研究工作. ORCID:0009-0002-4492-7599. E-mail: jiawenl96@126.com

* **通讯作者：**田世洪，E-mail: s.h.tian@163.com

引用格式：刘嘉文，田世洪，耿显雷，梁正伟，陈露，2024.俯冲沉积物交代造山带岩石圈地幔：来自三江地区煌斑岩钾同位素的约束.地球科学，49(11)：3930－3945.

Citation: Liu Jiawen, Tian Shihong, Geng Xianlei, Liang Zhengwei, Chen Lu, 2024. Subduction-Induced Sedimentary Metasomatism of Orogenic Lithospheric Mantle: Insights from Potassium Isotope in Lamprophyres of Sanjiang Region. *Earth Science*, 49(11): 3930－3945.

reveals that the lamprophyres from four distinct regions - Jianchuan, Beiya, Yanyuan, and Yao'an - collectively represent the characteristics of the mantle source. These samples exhibit no association with weathering alteration, fractional crystallization, crustal contamination, and dynamic fractionation processes. Overall, compared to the mantle, the samples display slightly lighter potassium isotopic compositions from (−0.61±0.02)‰ to (−0.31±0.01)‰, suggesting a correlation with subducted sediment metasomatism rather than with fluids typically enriched in heavier potassium isotopes. Further simulations utilizing the Monte Carlo model for end-member mixing calculations indicate varying degrees of subducted sediment incorporation in the four regions, with the sediment proportion in the Yao'an area potentially reaching up to 10%. This conclusion further substantiates the efficacy of potassium isotope as a sensitive tracer, capable of effectively tracking the recycled subduction sediment components within the mantle.

Key words: potassium; isotopes; sedimentary metasomatism; Sanjiang region; lamprophyres; orogenic lithospheric mantle; geochemistry.

钾质-超钾质火成岩是一类K_2O/Na_2O(>1)、K_2O和MgO含量均>3%的富钾幔源岩浆岩,这类岩石主要在板内环境和造山带环境(或后碰撞环境)中形成.例如,在东非大裂谷、环大西洋裂谷和我国东北地区的板内拉张裂谷环境中,它们表现出与地幔柱相关的洋岛玄武岩(OIB)型地球化学特征,暗示富钾物质可能来源于地幔深部,特别是在地幔过渡带(410~660 km)滞留的俯冲板片,但在阿尔卑斯-喜马拉雅造山带和我国三江地区等造山带环境(或后碰撞环境)中,这些岩石的微量元素整体呈现岛弧岩浆的特征,表明其地幔源区的交代通常与深度较浅(<200 km)的大洋或大陆板片俯冲有关(Turner *et al.*, 1996; Miller *et al.*, 1999; Zhao *et al.*, 2009; Gupta, 2015; Liu *et al.*, 2017; Soder and Romer, 2018; Wang *et al.*, 2021b).由于其独特的矿物学和地球化学特征,钾质-超钾质火成岩能够作为理想的"岩石探针",用于了解岩石圈地幔组成、揭示壳幔相互作用、构建地球动力学过程、探究大陆深俯冲以及Cu(-Mo-Au)等多金属矿床形成机制(Müller and Groves, 1993; Guo *et al.*, 2005; Prelević *et al.*, 2008; Zhao *et al.*, 2009; Lu *et al.*, 2015; Tian *et al.*, 2017; Soder and Romer, 2018; Liu *et al.*, 2021; Shen *et al.*, 2021, 2022).其岩石成因通常与富钾熔体或来自俯冲壳源物质的流体相关,这些熔体、流体与地幔相互作用形成了含角闪石或金云母的岩脉,随后通过板块折返、走滑断裂和岩石圈拆沉等一系列的构造作用发生部分熔融,从而形成钾质-超钾质火成岩(Foley, 1992; Prelević *et al.*, 2008; Soder and Romer, 2018; Förster *et al.*, 2019; Palmer *et al.*, 2019; Dalslåen *et al.*, 2020; Miao *et al.*, 2023).因此,俯冲板片来源的熔体或流体交代造山带岩石圈地幔被认为是钾质-超钾质火成岩的地幔源区(Gupta, 2015; Lu *et al.*, 2015; Soder and Romer, 2018; Palmer *et al.*, 2019; Liu *et al.*, 2021; Shen *et al.*, 2022; Miao *et al.*, 2023),但前人关于其地幔源区的研究仍存在争议性,例如,Murphy *et al.*(2002)用铅同位素对南极洲Gaussberg煌斑岩(幔源超钾质岩)的地幔源区进行了研究,认为其源区受俯冲至地幔过渡带或深部地幔的陆壳沉积物相关熔体的影响.富钾岩浆岩的主微量元素和放射性同位素特征通常与俯冲沉积物相似,可能代表再循环陆源沉积物使岩浆岩富集钾,但在富钾岩浆岩中,钾富集与指示沉积物的Sr-Nd-Pb同位素、Th/Nb、Sm/La等指标并无明显的相关性,暗示样品的主微量元素和放射性同位素可能无法有效识别出地幔源区再循环沉积物(Tommasini *et al.*, 2011; Prelević *et al.*, 2013; Wang *et al.*, 2021b).因此,需要一个新的示踪工具来识别地幔源区再循环的物质组分.

钾是陆壳(1.5%)的主要组成元素,在地幔中较少(240×10^{-6}, McDonough and Sun, 1995; Rudnick and Gao, 2014),作为主要造岩元素,具有$\delta^{39}K$(93.258%)和$\delta^{41}K$(6.730%)两种稳定同位素,其相对质量差高达5%.因此,在低温地质过程中钾同位素会产生显著的质量依赖分馏(Berglund and Wieser, 2011; Teng *et al.*, 2017),例如化学风化蚀变和成岩过程(Teng *et al.*, 2020; Wang *et al.*, 2021a; Huang *et al.*, 2023).然而,在部分熔融、岩浆分异这类高温地质过程中钾同位素不发生显著的分馏(Tuller-Ross *et al.*, 2019a, 2019b; Hu *et al.*, 2020, 2021b).第一性原理的计算也给出了类似的结论(Zeng *et al.*, 2019).前人研究表明,新鲜洋中脊玄武岩(MORB)和洋岛玄武岩(OIB)的$\delta^{41}K$值分别为(−0.44±0.17)‰、(−0.41±0.16)‰(Tuller-Ross *et al.*, 2019a),与地幔的$\delta^{41}K$值((−0.42±0.08)‰,Hu *et al.*, 2021b)在误差范围内基本一致.然而,蚀变洋

壳(AOC)由于经历了与海水((0.12±0.07)‰,Hille *et al.*, 2019; Wang *et al.*, 2020)的相互反应,其具有明显重于地幔的钾同位素组成(−1.07‰~0.01‰, Santiago Ramos *et al.*, 2020; Liu *et al.*, 2021).相比之下,俯冲沉积物的钾同位素组成具有较大的变化范围($\delta^{41}K$=−1.3‰~−0.02‰,Hu *et al.*, 2020),但整体(均值为−0.56‰,Hu *et al.*, 2020)显著低于地幔值((−0.42±0.08)‰,Hu *et al.*, 2021b).此外,钾作为大离子亲石元素和高度不相容元素,在俯冲变质脱水过程中大量的钾会被释放到板片相关的流体或超临界流体中(Liu *et al.*, 2021),因此,由大洋板片脱水而来的流体富集重钾同位素(0.13‰~1.37‰,Liu *et al.*, 2020).在岩浆结晶分异过程中,矿物(斜长石、黑云母等)的分离结晶也会使钾同位素产生分馏(Hu *et al.*, 2021b; Huang *et al.*, 2023).综上所述,钾同位素可用于示踪幔源岩浆地幔源区中再循环物质的性质及其来源.例如,我国东北地区的钾质玄武岩、喜马拉雅-青藏高原后碰撞造山带的富钾质岩和Lesser Antilles的弧火山岩均表现出显著低于地幔的轻钾同位素特征(分别为−0.81‰~−0.15‰、−1.55‰~−0.32‰和−0.66‰~0.01‰),指示这些岩浆的地幔源区有显著的俯冲沉积物或沉积物相关熔体的贡献(Sun *et al.*, 2020; Wang *et al.*, 2021b; Hu *et al.*, 2021a).我国北秦岭造山带宝鸡地区的超钾质岩表现出高于地幔((−0.42±0.08)‰,Hu *et al.*, 2021b)的重钾同位素特征(−0.57‰~−0.06‰),且与K/Th、Ba/Rb等流体相关指标具有正相关性,表明地幔源区有强烈俯冲板片相关流体交代的痕迹(Liu *et al.*, 2021).

青藏高原-喜马拉雅造山带广泛分布着始新世-渐新世后碰撞钾质-超钾质火成岩,这类岩石作为研究壳幔物质循环和相互作用的理想“探针”,备受地质学界的关注(Lu *et al.*, 2015).据此,本研究针对我国西南三江地区始新世-渐新世后碰撞煌斑岩的钾同位素开展了研究,并结合Geng *et al.*(2024)已发表的主微量元素和放射性同位素地球化学数据,旨在为碰撞后造山环境地幔源区再循环物质的识别提供新的证据.

1 地质背景和样品特征

1.1 地质背景

自新生代以来,印度板块和亚欧板块的相互碰撞形成了青藏高原-喜马拉雅造山带,该造山带是目前全球最大、最典型的大陆碰撞造山带,在特提斯域的地质构造中占据重要地位(Yin and Harrison, 2000).青藏高原经历了特提斯洋的复杂演化过程,主要由羌塘、拉萨、喜马拉雅和松潘-甘孜四大地块构成,这些地块之间由金沙江-哀牢山缝合带、班公湖-怒江缝合带、印度-雅鲁藏布江缝合带所界定(图1a, Yin and Harrison, 2000; Chung *et al.*, 2005; Pan *et al.*, 2012).我国西南三江地区(金沙江、澜沧江和怒江)位于青藏高原的东南缘,是青藏高原-喜马拉雅造山带的重要组成部分,同时也是扬子克拉通、思茅地块和印支地块的交汇部位(图1a, Deng *et al.*, 2014),该区域代表着古特提斯洋关闭后,由冈瓦纳大陆的微陆块和古生代弧地体的一系列拼贴而形成(Cocks and Torsvik, 2013; Deng *et al.*, 2014).此外,区域内构造演化历史较为复杂,拉张和挤压等构造活动频发,形成了数条缝合带、断裂带和多个微陆块(莫宣学等,2009).其北段以甘孜-理塘缝合线、龙门山断裂隔开了松潘-甘孜地块和羌塘地块,而南段则通过金沙江-哀牢山和昌宁-孟连缝合线分隔了扬子克拉通、思茅地块和保山地块(图1b).三江地区地层发育完整,在金沙江-哀牢山缝合线附近有元古界变质程度低的大理岩、片岩等岩石类型产出.在古生界-中生界时期,金沙江-红河断裂带的两侧均有碎屑岩和碳酸盐岩的沉积.在新生界时期,不同区域的岩性有很大的差异性,表明该时期区域构造活跃(Wang *et al.*, 2001).区域内也有新元古代变质基底,在扬子克拉通西缘新元古代还留有海底俯冲的痕迹(Zhao *et al.*, 2018; Zhu *et al.*, 2021).三江地区自新生代(~65 Ma)以来经历了多阶段的陆内变形,形成了一系列的褶皱带和走滑断裂带,特别是哀牢山−红河断裂带、金沙江断裂带均出露了大量的始新世-渐新世后碰撞钾质-超钾质火成岩(Xu *et al.*, 2001; Huang *et al.*, 2010; Gan and Huang, 2017),这些岩石与碰撞型斑岩Cu(-Mo-Au)等多金属矿床具有密切的时空关系(图1b).

1.2 样品特征

本研究的样品包含来自剑川、北衙、盐源和姚安4个地区的22件始新世-渐新世(大约30~40 Ma;Lu *et al.*, 2015)煌斑岩.我们之前的研究已对这些样品的岩相学特征、主微量元素和Sr-Nd-Pb同位素数据进行了详细报道(Geng *et al.*, 2024),这里做简要总结.样品均具有斑状结构,主要由金云

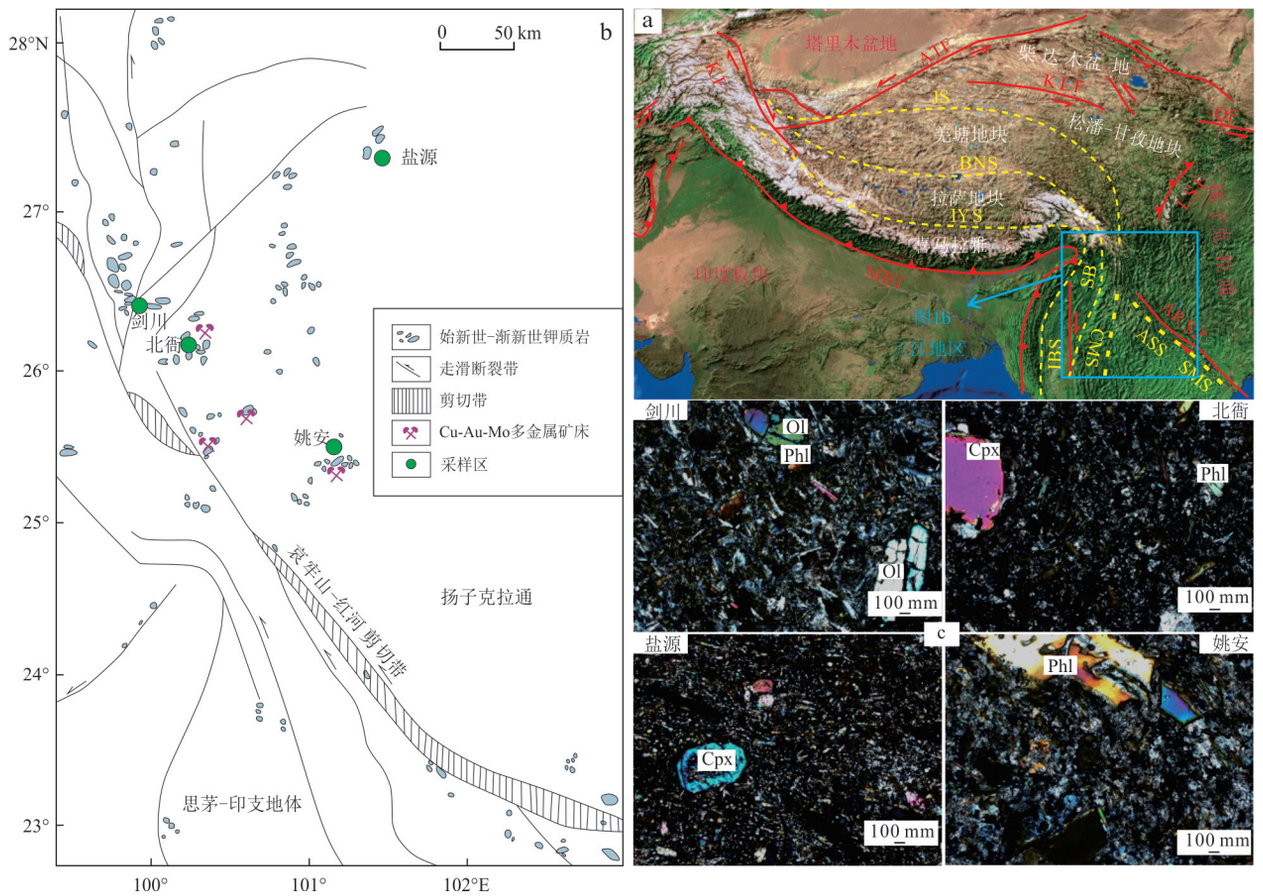

图 1　青藏高原及三江地区构造格架示意(a.据 Yin and Harrison, 2000; Chung *et al.*, 2005; Shen *et al.*, 2021; Geng *et al.*, 2024 修改),三江地区始新世-渐新世钾质岩的分布(b.据 Guo *et al.*, 2005; Deng *et al.*, 2014; Miao *et al.*, 2023 修改)和三江地区煌斑岩的显微镜下照片(c)

Fig. 1　Schematic of the tectonic framework of the Tibetan plateau and the Sanjiang region (a, modified after Yin and Harrison, 2000; Chung *et al.*, 2005; Shen *et al.*, 2021; Geng *et al.*, 2024), distribution of Eocene-Oligocene potassic rocks in the Sanjiang region (b, modified after Guo *et al.*, 2005; Deng *et al.*, 2014; Miao *et al.*, 2023) and representative photomicrographs of lamprophyres from the Sanjiang region (c)

JS.金沙江缝合带;BNS.班公湖-怒江缝合带;IYS.印度河-雅鲁藏布江缝合带;MBT.主边界逆冲断裂;ARSZ.哀牢山-红河剪切带;KF.喀喇昆仑断裂带;ATF.阿尔金断裂带;KLF.昆仑断裂带;QF.秦岭断裂带;LSF.龙门山断裂带;IBS.印度-缅甸缝合带;SB.山界;CMS.昌宁-孟连缝合带;ASS.哀牢山缝合带;SMS.Song Ma缝合带;Phl.金云母;Cpx.单斜辉石;Ol.橄榄石

母、橄榄石和单斜辉石等矿物组成,矿物的颗粒大小不一,以自形和半自形的形式存在.金云母主要为针状和板状,橄榄石主要为粒状和柱状,部分含有大块橄榄石巨晶.单斜辉石呈卵状,呈现出明显的核边结构(图 1c).副矿物有少量的磷灰石、钛铁矿等.全岩主微量元素显示样品具有高 K_2O(4.00%~8.27%)和低 SiO_2(41.57%~60.60%)及 K_2O+Na_2O(6.77%~10.74%)(表 1),在 TAS 图解中落在碱玄岩-粗面岩范围内,属于中基性岩(图 2a).在 SiO_2-Na_2O 图解中,样品落在了钾玄质和超钾质系列范围内,且 K_2O/Na_2O 均大于 1,为钾质和超钾质岩类(图 2b).原始地幔标准化微量元素蛛网图呈现出样品的 LILE(K、Rb 和 Ba 等)富集,HFSE(Nb、Ta 和 Ti 等)亏损,Pb 具有正异常(图 2c).球粒陨石标准化稀土元素配分图显示样品富集 LREE,亏损 HREE,具有微弱的 Eu 负异常,表明样品与俯冲环境有关,相似于洋岛玄武岩(OIB),但与洋中脊玄武岩(MORB)明显不一致(图 2d, Sun and McDonough, 1989).

2　分析方法

钾同位素的实验全流程在东华理工大学金属同位素与铀多金属成矿作用实验室完成.化学前处理流程:(1)称取 10~55 mg 的全岩样品粉末(<200

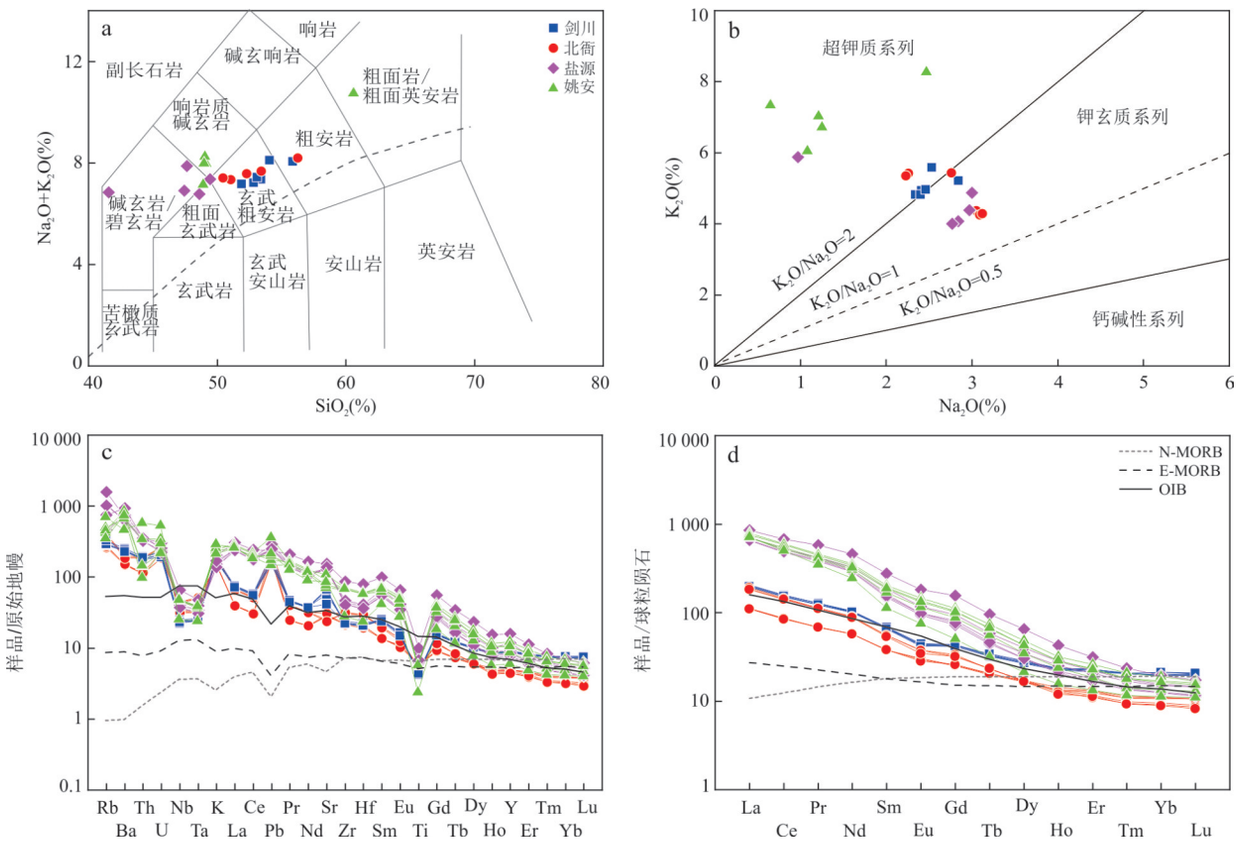

图 2 三江地区煌斑岩(Na_2O+K_2O)-SiO_2分类命名图解,其中灰色虚线为碱性(上部)和亚碱性(下部)系列的分界线(a. Irvine and Baragar, 1971)、K_2O-Na_2O系列判别图解(b)、微量元素原始地幔标准化蛛网图(c)和稀土元素球粒陨石标准化配分图(d)

Fig. 2 Classification diagram of Na_2O+K_2O vs. SiO_2, with the gray dashed line dividing the alkaline (above) and sub-alkaline (below) fields (a, Irvine and Baragar, 1971), K_2O vs. Na_2O diagram (b), primitive mantle-normalized incompatible element patterns (c), and chondrite-normalized REE patterns for lamprophyres from the Sanjiang region (d)

图 a 和 b 底图分别引自 Middlemost(1994)和 Le Maitre(2002),剑川、北衙、盐源和姚安煌斑岩数据引自 Geng *et al.* (2024),N-MORB、E-MORB、OIB 引自前人数据(Sun and McDonough, 1989)

目)至 15 mL Savillex PFA 材质的烧杯中,向杯中加入二次蒸馏的浓 HNO_3和浓 HF (体积比为 1∶3),拧紧盖子摇匀,置于 120 ℃的电热板加热 48 h;(2)冷却后将上述混酸蒸干,加入 1 mL 二次蒸馏的浓 HNO_3反应后再次蒸干;(3)加入 2 mL 王水放置在 120 ℃电热板上加热至溶液清澈透明;(4)继续蒸干样品溶液,用 1.0 mol/L HNO_3溶解样品使得钾的浓度为 40 μg/mL,以备后续过柱;(5)过柱前填充~3 mL 200~400 目 BioRad® AG50W-X8 树脂,并使用 MQ 水、6 mol/L HCL 和 1 mol/L HNO_3上柱清洗树脂;(6)上样体积为 1 mL,使用混酸(1 mol/L HNO_3+0.1 mol/L HF)去除基质元素(例如,Ti,Na,Al),然后使用 0.7 mol/L HNO_3接收钾溶液.钾的回收率大于 99%.

上机测试所用仪器为英国 Nu 公司所生产的 sapphire 多接收电感耦合等离子体质谱仪(CC-MC-ICP-MS),该型号质谱仪带有碰撞反应池,具有双路径,能够较大程度减少 ArH^+对 $^{41}K^+$的干扰.将过完柱子的纯钾溶液放置 110 ℃的加热板蒸干,之后溶于 2% HNO_3中,并用同一配制的 2% HNO_3将每个样品和标样浓度稀释至 200×10^{-9},在仪器测试时使用样品-标样交叉法(SSB)校正质量歧视效应.在法拉第杯 H2 和 L5 接收 ^{41}K 和 ^{39}K 的信号值.钾同位素通常以 $\delta^{41}K$ 方式表示,其计算公式为 $\delta^{41}K=[(^{41}K/^{39}K)_{样品}/(^{41}K/^{39}K)_{标样}-1]\times10^3$,其中基准标样为 NIST SRM 3141a.根据对纯钾溶液 A-K 的长期监测,可以确定外部重现性优于 0.05‰.此外,整个实验流程采用国际标样 AGV-2 和 BCR-2 作为监控标样,其钾同位素测试值分别为 $\delta^{41}K=(-0.47\pm0.03)$‰ (2SD, $n=10$)和 $\delta^{41}K=(-0.45\pm0.04)$‰(2SD, $n=10$),与前人报道的 AGV-2((-0.47 ± 0.03)‰, $n=8$, Chen *et al.*, 2021)和 BCR-2((-0.45 ± 0.03)‰, $n=5$, Chen *et al.*, 2021)的 $\delta^{41}K$ 值在误差范围内

一致,全流程空白低于 0.3 ng.

3　钾同位素特征

全岩样品的 $\delta^{41}K$ 值在(−0.61±0.02)‰～(−0.31±0.01)‰(表 1),变化范围大于地幔值((−0.42±0.08)‰,Hu *et al.*, 2021b).这些样品的钾同位素与我国西南小纪罗和南板桥碱性钾质岩($\delta^{41}K$ = −0.56‰～−0.30‰,Miao *et al.*, 2023)、土耳其安纳托利亚造山带钾玄质-超钾质岩($\delta^{41}K$ = −0.55‰～−0.32‰,Du *et al.*, 2024)的变化范围相似,它们均在阿尔卑斯-喜马拉雅造山带钾质-超钾质火山岩(−1.55‰～−0.32‰,Wang *et al.*, 2021b)、中国东北玄武质熔岩(−0.81‰～−0.15‰,Sun *et al.*, 2020)和 Lesser Antilles 弧火山岩(−0.66‰～0.01‰,Hu *et al.*, 2021a)的 $\delta^{41}K$ 值变化范围内,而与我国北秦岭造山带宝鸡超钾质岩的 $\delta^{41}K$ 值(−0.57‰～−0.06‰,Liu *et al.*, 2021)和西南卓潘碱性岩的 $\delta^{41}K$ 值(−0.42‰～0.48‰,Miao *et al.*, 2023)明显不同(图 3).

4　讨论

前人的研究表明三江地区的这些钾质-超钾质火成岩是富金云母交代岩石圈地幔部分熔融和结晶分异的产物(Geng *et al.*, 2024 及其参考文献).在讨论地幔源区钾同位素特征之前,还需要评估低温蚀变、地壳混染、结晶分异、动力学分馏等地质过程对所研究煌斑岩样品钾同位素组成的影响.

4.1　风化蚀变和地壳混染

在风化蚀变过程中,重钾同位素倾向于进入流体相,而轻钾同位素优先残留在风化产物中,即化学风化过程会影响火成岩的钾同位素组成,使 $\delta^{41}K$ 值变低(Li *et al.*, 2019a; Chen *et al.*, 2020; Huang *et al.*, 2020; Sun *et al.*, 2020; Teng *et al.*, 2020).本研究采集的 22 件煌斑岩样品在实验前进行了严

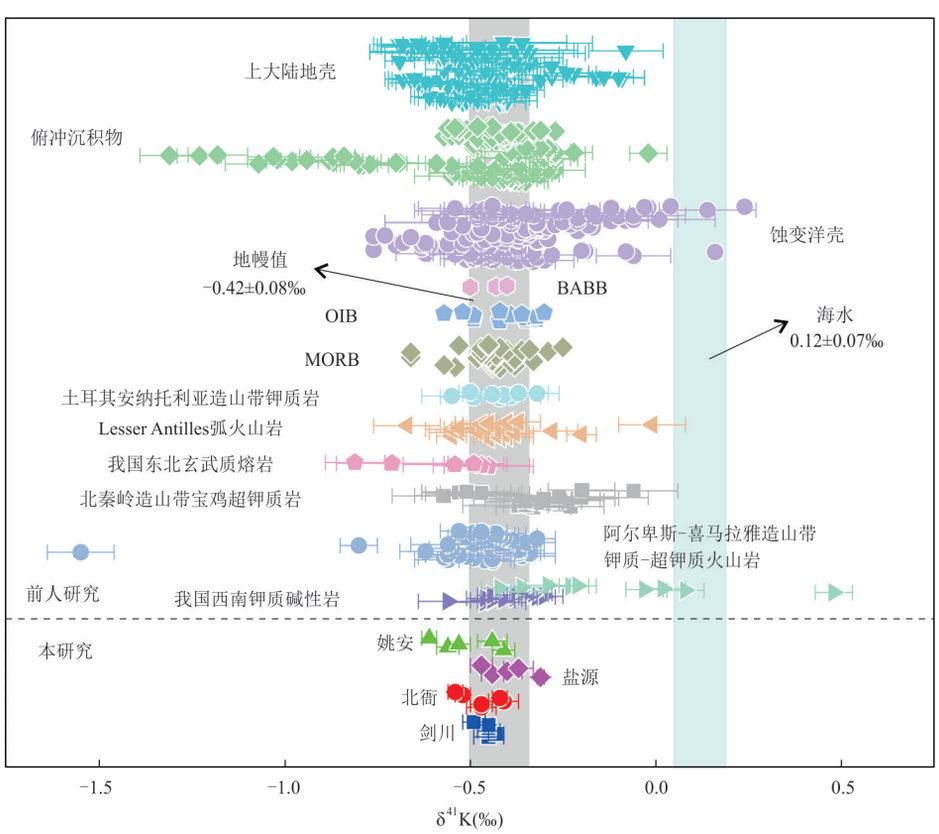

图 3　三江地区煌斑岩样品与前人报道的不同地区岩浆岩样品的钾同位素变化

Fig. 3　Potassium isotope variation diagram comparing lamprophyres from the Sanjiang region with magmatic rocks from different areas as previously reported

前人数据引自文献(Parendo *et al.*, 2017; Hille *et al.*, 2019; Li *et al.*, 2019b, 2022, 2024; Tuller-Ross *et al.*, 2019a; Hu *et al.*, 2020, 2021a; Huang *et al.*, 2020, 2023; Santiago Ramos *et al.*, 2020; Sun *et al.*, 2020; Wang *et al.*, 2020, 2021b; Liu *et al.*, 2021; Miao *et al.*, 2023; Du *et al.*, 2024)

格筛选，显微镜下观察发现样品整体较新鲜仅有轻微橄榄石蛇纹石化和黑云母绿泥石化(图1c).尽管样品的烧失量(LOI)变化范围较大(0.90%～7.64%)，可能反映不同程度的风化蚀变作用，但这些煌斑岩的$\delta^{41}K$值与LOI之间并没有相关性(图4a)，表明风化蚀变不是样品钾同位素变化的主要原因.

岩浆上升和侵位过程中地壳物质混染可能会改变幔源岩浆的钾同位素组成(Sun *et al.*, 2020).虽然大陆地壳的钾同位素组成范围(－0.68‰～－0.12‰, Huang *et al.*, 2020)与所研究煌斑岩的钾同位素组成有重叠，但以下证据表明地壳混染对所研究样品的钾同位素组成影响较小.首先，这些煌斑岩的K_2O含量(4.00%～8.27%，均值为5.37%)远高于大陆地壳(K_2O为1.8%，Rudnick and Gao, 2014)，使其钾同位素难以被地壳混染改变.其次，我们的计算表明要使具有正常地幔钾同位素组成的富钾质岩浆具有所研究煌斑岩的钾同位素组成，至少需要10%～30%的地壳物质混入(图5a)，这与样品的高MgO、$Mg^{\#}$、Cr和Ni含量不符(表1).另外，这些煌斑岩的Sr-Nd-Pb和K同位素与SiO_2之间缺乏明显的相关性(图4b～4e)，也进一步表明地壳混染作用不显著.

表1 三江地区煌斑岩主量元素(%)、微量元素(10^{-6})和Sr-Nd-Pb-K同位素(‰)地球化学分析测试结果

Table 1 Whole-rock major elements (%), trace elements (10^{-6}) and Sr-Nd-Pb-K isotopes (‰) geochemical analysis results of lamprophyres from the Sanjiang region

样品编号	MgO	SiO_2	K_2O	Al_2O_3	CaO	K_2O/Na_2O	K_2O+Na_2O	$Mg^{\#}$	LOI	Cr	Ni	Rb/Sr	Ba/Rb	K/Th
JC20-3-1	3.96	51.9	4.83	12.27	7.45	2.06	7.17	0.50	7.51	57	31	0.13	9.24	2 864
JC20-3-2	4.68	53.4	4.95	12.46	6.79	2.05	7.35	0.53	5.05	56	37	0.14	8.66	2 959
JC20-3-3	5.12	54.1	5.59	13.33	5.65	2.21	8.11	0.54	2.78	69	32	0.17	8.41	3 027
JC20-3-4	4.99	52.8	4.83	12.40	6.62	2.02	7.22	0.53	5.17	59	37	0.13	8.87	2 817
JC20-3-5	4.53	53.1	4.97	12.54	6.86	2.02	7.44	0.51	4.81	54	31	0.13	9.02	2 908
JC20-3-6	3.92	55.9	5.22	13.67	6.13	1.84	8.06	0.50	2.34	61	33	0.24	7.56	2 929
BY20-1-3	6.30	56.3	5.44	14.03	3.86	1.97	8.20	0.67	2.75	225	171	0.47	5.45	3 183
BY20-1-4	5.97	50.4	4.37	14.02	7.51	1.43	7.42	0.60	4.71	259	158	0.30	5.96	4 058
BY20-1-5	5.84	51.1	4.25	13.83	6.92	1.37	7.35	0.61	5.69	253	159	0.27	6.25	3 989
BY20-1-6	5.79	50.4	4.29	14.16	7.07	1.37	7.42	0.61	5.22	258	158	0.28	6.18	3 894
BY20-1-7	5.74	53.4	5.43	13.17	5.22	2.40	7.68	0.66	6.59	254	167	0.39	5.60	3 035
BY20-1-8	5.93	52.3	5.35	12.94	5.90	2.40	7.58	0.68	7.64	239	159	0.50	5.21	2 955
YY20-2-1	8.25	49.5	4.39	12.72	9.41	1.48	7.36	0.68	0.98	363	254	0.11	17.95	1 246
YY20-2-2	8.83	47.4	4.07	12.02	10.64	1.43	6.92	0.69	1.63	397	277	0.36	4.78	1 330
YY20-2-3	8.76	48.6	4.00	12.44	9.67	1.45	6.77	0.68	1.25	355	257	0.25	6.58	1 156
YY20-2-4	13.04	41.6	5.88	8.45	12.22	6.07	6.85	0.76	2.16	564	474	0.15	13.72	1 734
YY20-2-5	8.87	47.6	4.88	11.92	10.48	1.62	7.88	0.69	0.90	394	282	0.22	6.81	1 574
YA20-1-1	6.01	49.2	6.71	11.27	8.09	5.35	7.96	0.63	6.04	142	60	0.18	18.67	7 290
YA20-1-2	6.67	49.0	7.02	11.17	8.32	5.79	8.24	0.66	6.06	163	67	0.17	14.80	2 179
YA20-1-3	6.25	49.0	7.33	11.35	7.90	11.29	7.97	0.63	5.74	145	60	0.12	20.97	5 463
YA20-1-6	6.23	48.9	6.05	11.35	8.55	5.60	7.13	0.64	6.61	151	62	0.14	23.35	4 389
YA20-1-7	2.04	60.6	8.27	15.45	2.73	3.35	10.74	0.47	2.58	78	29	0.25	7.26	1 514

样品编号	$^{87}Sr/^{86}Sr$	$^{143}Nd/^{144}Nd$	$^{206}Pb/^{204}Pb$	$^{207}Pb/^{204}Pb$	$^{208}Pb/^{204}Pb$	$\varepsilon_{Nd}(t)$	$\delta^{41}K$	2SD
JC20-3-1	0.708 125	0.512 398	18.693 9	15.650 2	38.841 6	－4.23	－0.45	0.04
JC20-3-2	0.708 084	0.512 392	18.695 9	15.649 8	38.843 2	－4.34	－0.43	0.02
JC20-3-3	0.708 159	0.512 399	18.688 4	15.651 0	38.838 7	－4.21	－0.45	0.03
JC20-3-4	0.708 127	0.512 383	18.701 9	15.650 2	38.850 0	－4.51	－0.45	0.00
JC20-3-5	0.708 099	0.512 388	18.691 2	15.650 8	38.839 9	－4.43	－0.45	0.01
JC20-3-6	0.708 540	0.512 353	18.713 3	15.657 0	38.881 2	－5.09	－0.49	0.03
BY20-1-3	0.708 669	0.512 388	18.667 8	15.712 3	39.142 9	－4.38	－0.47	0.04
BY20-1-4	0.706 739	0.512 579	18.680 0	15.709 3	39.143 8	－0.70	－0.47	0.03

续表 1

样品编号	$^{87}Sr/^{86}Sr$	$^{143}Nd/^{144}Nd$	$^{206}Pb/^{204}Pb$	$^{207}Pb/^{204}Pb$	$^{208}Pb/^{204}Pb$	$\varepsilon_{Nd}(t)$	$\delta^{41}K$	2SD
BY20-1-5	0.706 848	0.512 585	18.700 0	15.721 6	39.177 5	−0.58	−0.41	0.04
BY20-1-6	0.706 798	0.512 577	18.697 1	15.716 4	39.173 9	−0.74	−0.42	0.02
BY20-1-7	0.708 678	0.512 368	18.682 7	15.713 7	39.163 3	−4.78	−0.52	0.02
BY20-1-8	0.708 839	0.512 359	18.688 4	15.714 8	39.168 3	−4.95	−0.54	0.02
YY20-2-1	0.706 162	0.512 481	18.273 3	15.611 6	38.598 9	−2.49	−0.31	0.01
YY20-2-2	0.706 337	0.512 472	18.271 2	15.612 6	38.605 7	−2.66	−0.44	0.03
YY20-2-3	0.706 176	0.512 478	18.276 3	15.611 1	38.595 6	−2.59	−0.40	0.04
YY20-2-4	0.706 327	0.512 481	18.388 9	15.622 2	38.662 6	−2.56	−0.37	0.04
YY20-2-5	0.706 289	0.512 471	18.268 2	15.610 0	38.600 7	−2.68	−0.47	0.03
YA20-1-1	0.709 673	0.512 086	18.350 2	15.603 2	38.933 3	−10.22	−0.41	0.03
YA20-1-2	0.709 528	0.512 088	18.313 2	15.593 3	38.890 7	−10.20	−0.56	0.03
YA20-1-3	0.709 353	0.512 092	18.333 4	15.598 8	38.911 9	−10.11	−0.53	0.03
YA20-1-6	0.709 621	0.512 092	18.349 3	15.603 2	38.942 2	−10.13	−0.44	0.04
YA20-1-7	0.710 421	0.512 028	18.358 8	15.622 5	39.178 1	−11.27	−0.61	0.02

注:三江地区煌斑岩样品的主微量元素和放射性同位素地球化学数据引自 Geng *et al.*(2024).

4.2　结晶分异

三江地区煌斑岩的 SiO_2 与 Cr、Ni、MgO 和 CaO 含量之间显示出显著的相关关系(相关系数 R^2 分别为 0.820 1、0.826 4、0.758 6 和 0.701 2),表明橄榄石和单斜辉石的分离结晶过程在岩浆演化中发挥了作用(Geng *et al.*, 2024).由于钾在橄榄石和单斜辉石中极度不相容(Philpotts and Schnetzler, 1970),这些矿物的结晶分异带走的钾相对于整个岩浆体系来说极其微小,因此理论上不会显著改变残余岩浆的钾同位素组成(Tuller-Ross *et al.*, 2019a, 2019b; Hu *et al.*, 2021b; Wang *et al.*, 2021a).前人对连续结晶分异演化岩浆体系的研究也证实岩浆早期橄榄石和单斜辉石结晶分异过程中钾同位素分馏极其微小(Hu *et al.*, 2021b; Huang *et al.*, 2023).此外,前人的研究表明这些钾质-超钾质岩浆演化过程中可能存在少量富钾的金云母或黑云母的结晶分异(Geng *et al.*, 2024 及其参考文献).Zeng *et al.*(2019)理论研究表明,在温度为 900 ℃和 1 100 ℃的条件下,硅酸盐熔体与结晶矿物(金云母、钾长石等)的钾同位素分馏最高仅有 0.14‰ 和 0.10‰.而在岩浆演化晚期黑云母的结晶分异会对岩浆体系的钾同位素组成产生较大的影响(Hu *et al.*, 2021b; Huang *et al.*, 2023),例如,Hu *et al.*(2021b)通过瑞利分馏模拟结果表明黑云母的结晶会使钾同位素在矿物和熔体的分馏因子达 −0.25‰～0.02‰.然而,我们的结果显示所研究煌斑岩的钾同位素组成与金云母或黑云母结晶分异指标(如 K_2O/Na_2O 和 Rb/Sr)并没有明显的相关性(图 5b,5c).这一特征指示金云母或黑云母的结晶分异程度较低,即使有,也没有造成整个岩浆体系钾同位素组成的显著改变.另外,钾同位素与岩浆结晶分异指标(如 SiO_2、MgO 和 K_2O)之间并无明显相关关系(图 4b、4f 和图 5a),同样说明结晶分异作用没有改变这些煌斑岩的钾同位素组成.虽然斜长石的结晶分异也会造成钾同位素产生较大的分馏(Li *et al.*, 2019c, 2019d; Wang *et al.*, 2022b),但煌斑岩样品未表现出明显的 Eu 负异常,且钾同位素与 Al_2O_3 之间并未观察到明显的相关性(图 2 和图 5d),表明岩浆演化过程中斜长石的结晶分异并不显著,煌斑岩样品中几乎没有斜长石的存在,这也表明我们样品的钾同位素组成不受岩浆分异过程的影响.

4.3　动力学分馏

大量的研究表明稳定同位素若发生较大的分馏,可能与化学扩散相关的动力学分馏有密切关系(Richter *et al.*, 2014; Huang *et al.*, 2009; Zeng *et al.*, 2019),由浓度梯度引起的扩散叫化学扩散,即元素是由高浓度端向低浓度端扩散,因此,若钾是从钾质熔体中扩散到围岩或周围的地幔中,则样品的 K_2O 含量较低,且钾同位素较高,两者应该存在明显的负相关关系,而我们的样品中并没有出现这种关系(图 5a),表明化学扩散不是煌斑岩钾同位素分馏的主要因素.

综上所述,三江地区煌斑岩样品整体新鲜无明显蚀变,其钾同位素组成不受风化蚀变、地壳混染、分离结晶和动力学分馏的显著影响,因而更可能反映了地幔源区的特征.

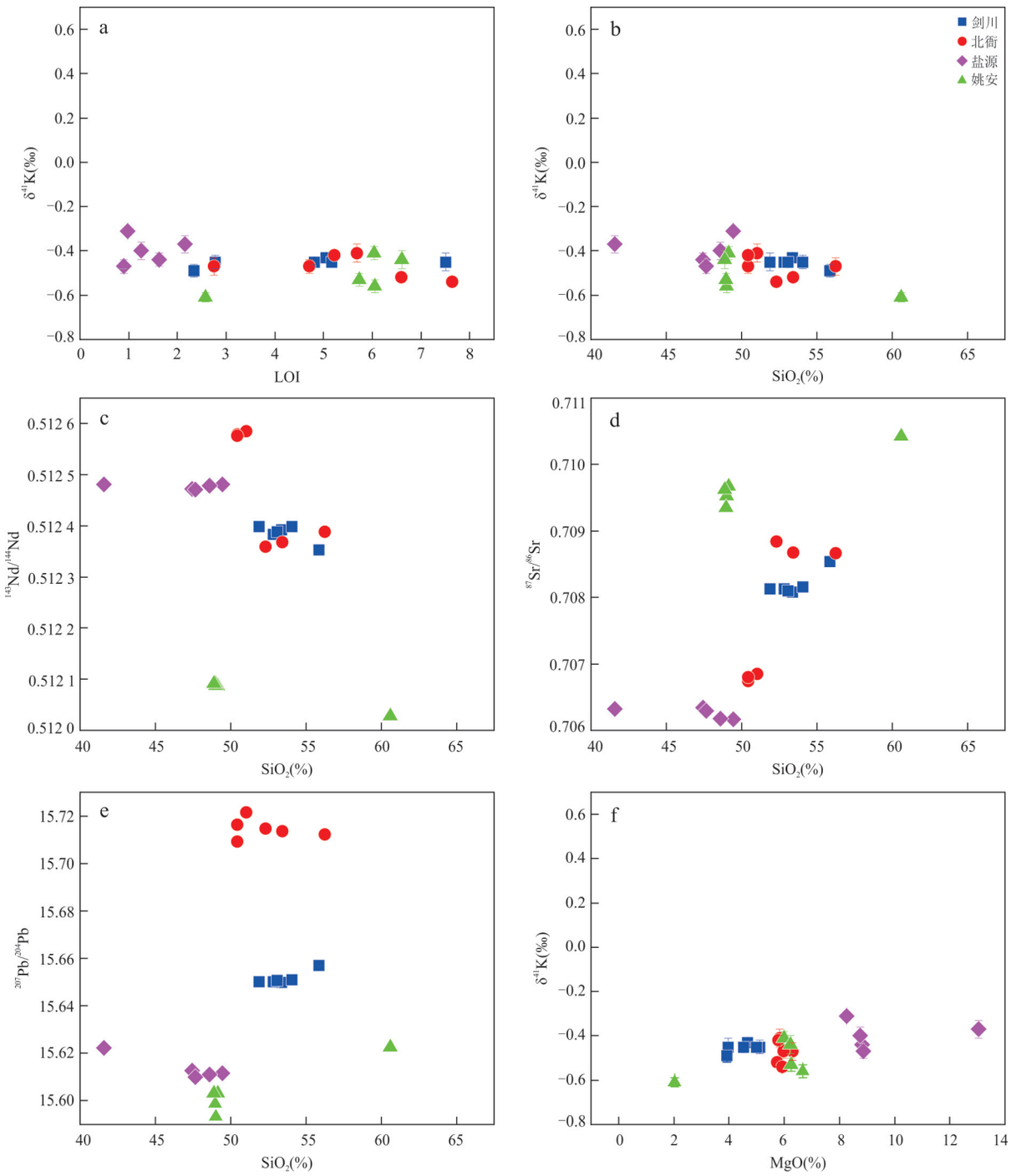

图 4 三江地区煌斑岩的 LOI 与 $\delta^{41}K$(a)、SiO_2 与 $\delta^{41}K$(b)、SiO_2 与 $^{143}Nd/^{144}Nd$(c)、SiO_2 与 $^{87}Sr/^{86}Sr$(d)、SiO_2 与 $^{207}Pb/^{204}Pb$(e)和 MgO 与 $\delta^{41}K$(f)关系

Fig.4 Plots of LOI vs. $\delta^{41}K$ (a), SiO_2 vs. $\delta^{41}K$ (b), SiO_2 vs. $^{143}Nd/^{144}Nd$ (c), SiO_2 vs. $^{87}Sr/^{86}Sr$ (d), SiO_2 vs. $^{207}Pb/^{204}Pb$ (e), and MgO vs. $\delta^{41}K$ (f) for lamprophyres from the Sanjiang region

4.4 钾同位素示踪地幔源区不均一性

三江地区煌斑岩样品的微量元素显示出弧岩浆岩的特征(富集 LILE,亏损 HFSE),这与俯冲作用的相关特征相吻合,可能受俯冲板片来源的富钾熔体或流体的交代(Geng *et al.*, 2024).前人研究发现蚀变洋壳、流体和俯冲沉积物三者在俯冲板片的钾循环中起主导作用,可能导致地幔源区钾同位素组成出现不均匀性(Wang *et al.*, 2021b; Wang and Ionov, 2023).相较于地幔($\delta^{41}K=(-0.42\pm0.08)‰$,Hu *et al.*, 2021b),蚀变洋壳和俯冲板片释放的流体

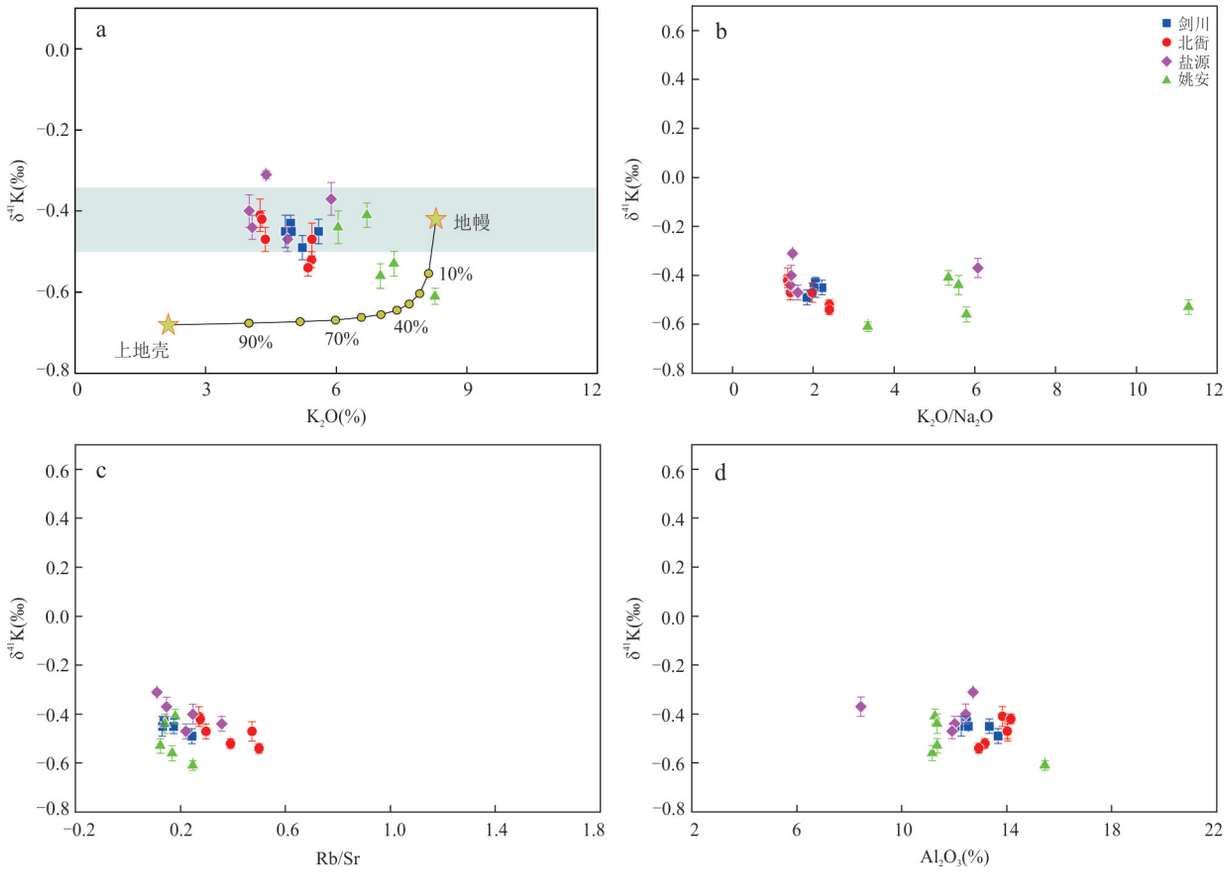

图 5　三江地区煌斑岩的 $\delta^{41}K$ 与 K_2O(a)、K_2O/Na_2O(b)、Rb/Sr(c)、Al_2O_3(d)关系

Fig.5　Plots of $\delta^{41}K$ vs. K_2O (a), K_2O/Na_2O (b), Rb/Sr (c), and Al_2O_3 (d) for lamprophyres from the Sanjiang region

图 a 模拟端元中,上地壳和富钾岩浆的 $\delta^{41}K$ 值分别为 −0.68‰ 和 −0.42‰(Huang *et al.*, 2020; Hu *et al.*, 2021b),K_2O 值分别为 2.14% 和 8.29%(Liu *et al.*, 2017)

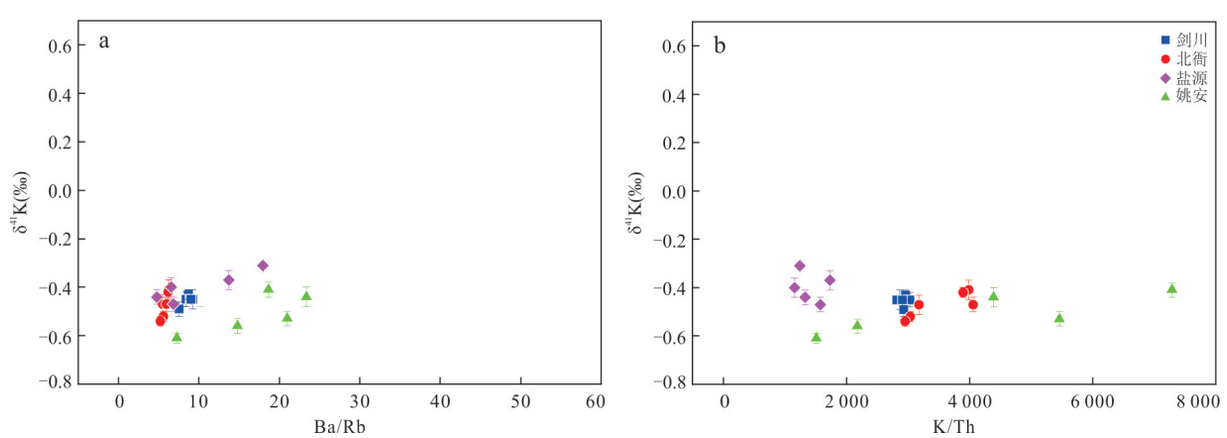

图 6　三江地区煌斑岩的 $\delta^{41}K$ 与 Ba/Rb(a)、K/Th(b)关系

Fig.6　Plots of $\delta^{41}K$ vs. Ba/Rb (a), and K/Th (b) for lamprophyres from the Sanjiang region

具有重钾同位素组成(−1.07‰～0.01‰、0.13‰～1.37‰, Santiago Ramos *et al.*, 2020; Hu *et al.*, 2020; Liu *et al.*, 2020),不可能使本研究煌斑岩样品产生较轻的钾同位素特征(−0.61‰～−0.31‰). 本研究样品的钾同位素组成与流体活动性指标(Ba/Rb、K/Th)之间没有相关性(图 6a,6b),并且蚀变洋壳的 $\varepsilon_{Nd}(t)$ 应具有正值,与我们样品的负 $\varepsilon_{Nd}(t)$ 值明显不同(Staudigel *et al.*, 1995; Wang *et al.*, 2021b),这表明煌斑岩低 $\delta^{41}K$ 值不是蚀变洋壳和俯冲流体交代地幔源区导致的,可能与俯冲相

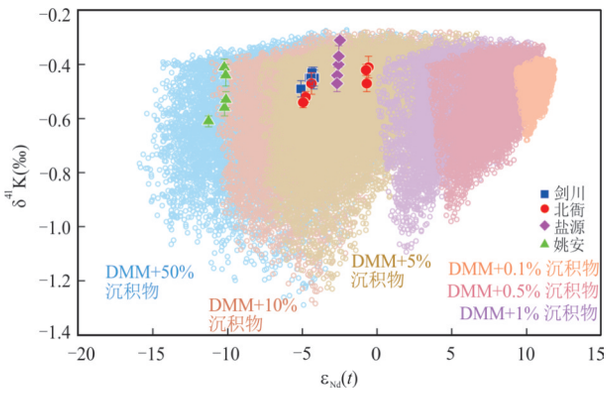

图 7 三江地区煌斑岩蒙特卡洛模型端元混合模拟

Fig. 7 Monte Carlo model end-member mixing simulation for lamprophyres from the Sanjiang region

我们运用蒙特卡洛模拟计算来进一步评估不同比例的沉积物对地幔源区钾同位素的影响.按照质量平衡,沉积物和地幔混合后的钾同位素组成计算公式为:$\delta^{41}K_{mix}=\{[K_2O]_{sediment}\times f\times\delta^{41}K_{sediment}+[K_2O]_{mantle}\times(1-f)\times\delta^{41}K_{mantle}\}/[K_2O]_{mix}$.其中$f$为混入地幔的沉积物比例,$\delta^{41}K_{sediment}$代表沉积物端元的钾同位素组成,数据来自于Hu *et al.*(2020);$\delta^{41}K_{mantle}$代表平均地幔组成,数据来源于Hu *et al.*(2021b).$\varepsilon_{Nd}(t)$的计算采用同样的方法计算得到.地幔和全球沉积物的钕同位素组成引用自Workman and Hart(2005)和Plank(2014).因沉积物钾同位素组成极为不均一,因此为了尽可能地表征沉积物端元的钾同位素组成,我们随机选择3个沉积物作为端元,按照随机的比例组成一个新的组合端元,计算出整个新的组合端元的钾和钕同位素组成,最后将新的组合端元的钾同位素和地幔混合,沉积物的混入比例为0.1%、0.5%、1%、5%、10%和50%来进行模拟计算,每个比例的沉积物与地幔的混合我们进行了10 000次的模拟,不同色彩的小圆圈构成的区域代表上述各个比例的沉积物和地幔混合后的钾同位素范围

关的沉积物或沉积物相关熔体有关(Hu *et al.*, 2020; Sun *et al.*, 2020; Wang *et al.*, 2021b),沉积物具有轻钾同位素组成(−1.3‰～−0.02‰)且$\varepsilon_{Nd}(t)$为负值(Hu *et al.*, 2020; Wang *et al.*, 2021b),最可能是造成地幔源区产生不均一性的原因,并且在俯冲进变质脱水过程中,沉积物中钾同位素不会产生明显的分馏(Wang *et al.*, 2022a),这表明俯冲沉积物的钾同位素特征可以代表煌斑岩的地幔源区特征.此外,俯冲沉积物的低$\delta^{41}K$值范围(−1.3‰～−0.02‰,Hu *et al.*, 2020)可以覆盖本研究所有煌斑岩样品的$\delta^{41}K$值(−0.61‰～−0.31‰),但剑川、北衙、盐源和姚安4个地区的钾同位素组成也有差异性,这表明地区之间的差异性可能源于不同比例的俯冲沉积物的影响.为了进一步评估俯冲沉积物对地幔源区的交代程度,本研究采用蒙特卡洛混合模型模拟了亏损地幔(DMM)和俯冲沉积物这两个端元的混合(图7),结果显示4个地区中,剑川、北衙和盐源3个地区的地幔源区有5%～10%俯冲沉积物的加入,而姚安地区地幔源区俯冲沉积物加入比例明显超过10%.综上所述,钾同位素是示踪地幔源区中沉积物组分的敏感指标.

在新元古代时期(1 000～900 Ma),沿扬子克拉通周缘发生了原特提斯洋的俯冲,形成了攀西-汉南弧岩浆带,这些弧岩浆有利于新生下地壳的形成.此外,俯冲沉积物交代三江地区煌斑岩的大陆岩石圈地幔源区,形成了不均一的富集岩石圈地幔(图8a).在晚始新世－渐新世时期(37～32 Ma),增厚的岩石圈地幔发生对流减薄,深部软流圈物质上涌,使岩石圈地幔发生不同程度的部分熔融,使得北衙、剑川、盐源和姚安地幔源区形成的富钾岩浆(煌斑岩)呈现出轻钾同位素特征(−0.61‰～−0.31‰,图8b),与三江思茅地块卓潘地区的钾质岩具有重钾同位素特征(−0.42‰～0.48‰)(Miao *et al.*, 2023)不一致,这也指示三江地区经历了复杂

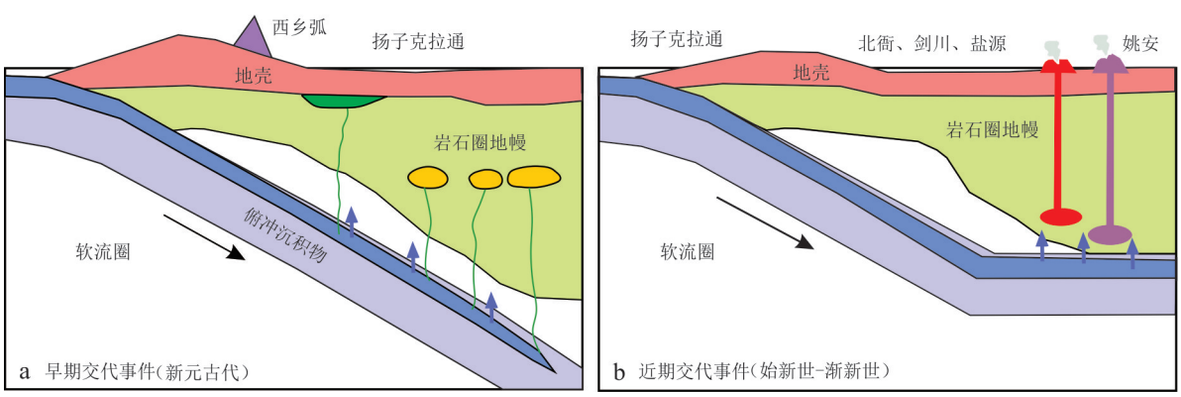

图 8 三江地区煌斑岩岩石圈地幔源区改造示意(据Lu *et al.*, 2013; Shen *et al.*, 2021; Sun *et al.*, 2021修改)

Fig. 8 Schematic diagrams of the lithospheric mantle source modification for lamprophyres from the Sanjiang region (modified after Lu *et al.*, 2013; Shen *et al.*, 2021; Sun *et al.*, 2021)

的构造演化过程,包括多重的碰撞和俯冲事件.

5　结论

(1)三江地区煌斑岩样品的钾同位素组成不受风化蚀变、地壳混染、分离结晶和动力学分馏的显著影响,表明其能够代表岩石圈地幔源区特征.

(2)三江地区煌斑岩样品的钾同位素组成变化范围在－0.61‰～－0.31‰,部分样品明显低于地幔钾同位素平均值,表明其岩石圈地幔主要受俯冲沉积物的交代,而不是俯冲流体.

(3)蒙特卡洛模拟计算表明,剑川、北衙和盐源3个地区的地幔源区有5%～10%俯冲沉积物的加入,而姚安地区地幔源区有>10%的俯冲沉积物交代.这也验证了钾同位素是示踪地幔源区中沉积物组分的敏感指标.

致谢:衷心感谢编辑部老师和审稿专家对本文提出的宝贵修改意见和指导!

References

Berglund, M., Wieser, M. E., 2011. Isotopic Compositions of the Elements 2009 (IUPAC Technical Report). *Pure and Applied Chemistry*, 83(2): 397－410. https://doi.org/10.1351/pac-rep-10-06-02

Chen, H., Liu, X. M., Wang, K., 2020. Potassium Isotope Fractionation during Chemical Weathering of Basalts. *Earth and Planetary Science Letters*, 539: 116192. https://doi.org/10.1016/j.epsl.2020.116192

Chen, H., Saunders, N. J., Jerram, M., et al., 2021. High-Precision Potassium Isotopic Measurements by Collision Cell Equipped MC-ICP-MS. *Chemical Geology*, 578: 120281. https://doi. org/10.1016/j. chemgeo.2021.120281

Chung, S. L., Chu, M. F., Zhang, Y. Q., et al., 2005. Tibetan Tectonic Evolution Inferred from Spatial and Temporal Variations in Post-Collisional Magmatism. *Earth-Science Reviews*, 68(3/4): 173－196. https://doi. org/10.1016/j.earscirev.2004.05.001

Cocks, L. R. M., Torsvik, T. H., 2013. The Dynamic Evolution of the Palaeozoic Geography of Eastern Asia. *Earth-Science Reviews*, 117: 40－79. https://doi.org/10.1016/j.earscirev.2012.12.001

Dalslåen, B. H., Gasser, D., Grenne, T., et al., 2020. Ordovician Shoshonitic to Ultrapotassic Volcanism in the Central Norwegian Caledonides: The Result of Sediment Subduction, Mantle Metasomatism and Mantle Partial Melting. *Lithos*, 356: 105372. https://doi. org/10.1016/j.lithos.2020.105372

Deng, J., Wang, Q. F., Li, G. J., et al., 2014. Cenozoic Tectono-Magmatic and Metallogenic Processes in the Sanjiang Region, Southwestern China. *Earth-Science Reviews*, 138: 268－299. https://doi.org/10.1016/j.earscirev.2014.05.015

Du, D. H., Luo, X. L., Wang, X. L., et al., 2024. A Recipe for Making Potassium-Rich Magmas in Collisional Orogens: New Insights from K and Fe Isotopes. *Earth and Planetary Science Letters*, 632: 118642. https://doi.org/10.1016/j.epsl.2024.118642

Foley, S., 1992. Vein-Plus-Wall-Rock Melting Mechanisms in the Lithosphere and the Origin of Potassic Alkaline Magmas. *Lithos*, 28(3/4/5/6): 435－453. https://doi.org/10.1016/0024-4937(92)90018-T

Förster, M. W., Buhre, S., Xu, B., et al., 2019. Two-Stage Origin of K-Enrichment in Ultrapotassic Magmatism Simulated by Melting of Experimentally Metasomatized Mantle. *Minerals*, 10(1): 41. https://doi. org/10.3390/min10010041

Gan, T., Huang, Z. L., 2017. Platinum-Group Element and Re-Os Geochemistry of Lamprophyres in the Zhenyuan Gold Deposit, Yunnan Province, China: Implications for Petrogenesis and Mantle Evolution. *Lithos*, 282: 228－239. https://doi.org/10.1016/j.lithos.2017.03.018

Geng, X. L., Tian, S. H., Xu, W., et al., 2024. A Two-Stage Geodynamic Model for Post-Collisional Potassic-Ultrapotassic Magmatism in Southeast Tibet. *Journal of Geophysical Research* (*Solid Earth*), 129(8): e2024JB028887. https://doi.org/10.1029/2024JB028887

Guo, Z. F., Hertogen, J., Liu, J. Q., et al., 2005. Potassic Magmatism in Western Sichuan and Yunnan Provinces, SE Tibet, China: Petrological and Geochemical Constraints on Petrogenesis. *Journal of Petrology*, 46(1): 33－78. https://doi.org/10.1093/petrology/egh061

Gupta, A. K., 2015. Origin of Potassium-Rich Silica-Deficient Igneous Rocks. Springer New Delhi, India, https://doi.org/10.1007/978-81-322-2083-1

Hille, M., Hu, Y., Huang, T.Y., et al., 2019. Homogeneous and Heavy Potassium Isotopic Composition of Global Oceans. *Science Bulletin*, 64(23): 1740－1742. https://doi.org/10.1016/j.scib.2019.09.024

Hu, Y., Teng, F. Z., Chauvel, C., 2021a. Potassium Isotopic Evidence for Sedimentary Input to the Mantle Source of Lesser Antilles Lavas. *Geochimica et Cosmochimica Acta*, 295: 98－111. https://doi. org/10.1016/j.gca.2020.12.013

Hu, Y., Teng, F. Z., Helz, R. T., et al., 2021b. Potassium Isotope Fractionation during Magmatic Differentiation and the Composition of the Mantle. *Journal of Geophysical Research* (*Solid Earth*), 126(3): e2020JB021543. https://doi.org/10.1029/2020JB021543

Hu, Y., Teng, F.Z., Plank, T., et al., 2020. Potassium Isotopic Heterogeneity in Subducting Oceanic Plates. *Science Advances*, 6(49): eabb2472. https://doi: 10.1126/sciadv.abb2472

Huang, X. L., Niu, Y. L., Xu, Y. G., et al., 2010. Mineralogical and Geochemical Constraints on the Petrogenesis of Post‐Collisional Potassic and Ultrapotassic Rocks from Western Yunnan, SW China. *Journal of Petrology*, 51(8): 1617—1654. https://doi.org/10.1093/petrology/egq032

Huang, F., Lundstrom, C. C., Glessner, J., et al., 2009. Chemical and Isotopic Fractionation of Wet Andesite in a Temperature Gradient: Experiments and Models Suggesting a New Mechanism of Magma Differentiation. *Geochimica et Cosmochimica Acta*, 73(3): 729—749. https://doi.org/10.1016/j.gca.2008.11.012

Huang, T. Y., Teng, F. Z., Rudnick, R. L., et al., 2020. Heterogeneous Potassium Isotopic Composition of the Upper Continental Crust. *Geochimica et Cosmochimica Acta*, 278: 122—136. https://doi. org/10.1016/j.gca.2019.05.022

Huang, T. Y., Teng, F. Z., Wang, Z. Z., et al., 2023. Potassium Isotope Fractionation during Granitic Magmatic Differentiation: Mineral‐Pair Perspectives. *Geochimica et Cosmochimica Acta*, 343: 196—211. https://doi.org/10.1016/j.gca.2022.11.006

Irvine, T. N., Baragar, W. R. A., 1971. A Guide to the Chemical Classification of the Common Volcanic Rocks. *Canadian Journal of Earth Sciences*, 8(5): 523—548. https://doi.org/10.1139/e71-055

Le Maitre, R.W., 2002. Igneous Rocks: A Classification and Glossary of Terms: Recommendations of the International Union of Geological Sciences Subcommission on the Systematics of Igneous Rocks. Cambridge University Press, Cambridge, 1—208. https://doi. org/10.1017/CBO9780511535581

Li, S. L., Li, W. Q., Beard, B. L., et al., 2019a. K Isotopes as a Tracer for Continental Weathering and Geological K Cycling. *Proceedings of the National Academy of Sciences of the United States of America*, 116(18): 8740—8745. https://doi.org/10.1073/pnas.1811282116

Li, W. Q., Li, S. L., Beard, B. L., 2019b. Geological Cycling of Potassium and the K Isotopic Response: Insights from Loess and Shales. *Acta Geochimica*, 38(4): 508—516. https://doi.org/10.1007/s11631-019-00345-x

Li, Y. H., Wang, W. Z., Huang, S. C., et al., 2019c. First-Principles Investigation of the Concentration Effect on Equilibrium Fractionation of K Isotopes in Feldspars. *Geochimica et Cosmochimica Acta*, 245: 374—384. https://doi.org/10.1016/j.gca.2018.11.006

Li, Y. H., Wang, W. Z., Wu, Z. Q., et al., 2019d. First-Principles Investigation of Equilibrium K Isotope Fractionation among K-Bearing Minerals. *Geochimica et Cosmochimica Acta*, 264: 30—42. https://doi. org/10.1016/j.gca.2019.07.038

Li, W. S., Coogan, L. A., Wang, K., et al., 2024. Hydrothermal Origin of Heavy Potassium Isotope Compositions in Altered Oceanic Crust: Implications for Tracing the Elemental Cycle. *Earth and Planetary Science Letters*, 625: 118448. https://doi. org/10.1016/j.epsl.2023.118448

Li, W. S., Liu, X. M., Wang, K., et al., 2022. Potassium Isotope Signatures in Modern Marine Sediments: Insights into Early Diagenesis. *Earth and Planetary Science Letters*, 599: 117849. https://doi. org/10.1016/j.epsl.2022.117849

Liu, D., Zhao, Z.D., Depaolo, D.J., et al., 2017. Potassic Volcanic Rocks and Adakitic Intrusions in Southern Tibet: Insights into Mantle‐Crust Interaction and Mass Transfer from Indian Plate. *Lithos*, 268—271: 48—64. https://doi: 10.1016/j.lithos.2016.10.034

Liu, H. Y., Wang, K., Sun, W. D., et al., 2020. Extremely Light K in Subducted Low-T Altered Oceanic Crust: Implications for K Recycling in Subduction Zone. *Geochimica et Cosmochimica Acta*, 277: 206—223. https://doi.org/10.1016/j.gca.2020.03.025

Liu, H. Y., Xue, Y. Y., Wang, K., et al., 2021. Contributions of Slab-Derived Fluids to Ultrapotassic Rocks Indicated by K Isotopes. *Lithos*, 396: 106202. https://doi.org/10.1016/j.lithos.2021.106202

Lu, Y. J., Kerrich, R., McCuaig, T. C., et al., 2013. Geochemical, Sr-Nd-Pb, and Zircon Hf-O Isotopic Compositions of Eocene‐Oligocene Shoshonitic and Potassic Adakite-Like Felsic Intrusions in Western Yunnan, SW China: Petrogenesis and Tectonic Implications. *Journal of Petrology*, 54(7): 1309—1348. https://doi. org/10.1093/petrology/egt013

Lu, Y. J., McCuaig, T.C., Li, Z. X., et al., 2015. Paleogene Post‐Collisional Lamprophyres in Western Yunnan, Western Yangtze Craton: Mantle Source and Tectonic Implications. *Lithos*, 233: 139—161. https://doi.

org/10.1016/j.lithos.2015.02.003

McDonough, W., Sun, S. S., 1995. The Composition of the Earth. *Chemical Geology*, 120: 223－253. https://doi.org/10.1016/0009-2541(94)00140-4

Miao, Z., Li, X. Q., Zhao, Z. D., et al., 2023. Deciphering Mantle Heterogeneity Associated with Ancient Subduction-Related Metasomatism: Insights from Mg-K Isotopes in Potassic Alkaline Rocks. *Geochimica et Cosmochimica Acta*, 348: 258－277. https://doi. org/10.1016/j.gca.2023.03.020

Middlemost, E. A. K., 1994. Naming Materials in the Magma/Igneous Rock System. *Earth-Science Reviews*, 37(3/4): 215－224. https://doi.org/10.1016/0012-8252(94)90029-9

Miller, C., Schuster, R., Klötzli, U., et al., 1999. Post-Collisional Potassic and Ultrapotassic Magmatism in SW Tibet: Geochemical and Sr-Nd-Pb-O Isotopic Constraints for Mantle Source Characteristics and Petrogenesis. *Journal of Petrology*, 40(9): 1399－1424. https://doi.org/10.1093/petroj/40.9.13999

Mo, X.X., Zhao, Z.D., Zhu, D.C., et al., 2009. On the Lithosphere of Indo‐Asia Collision Zone in Southern Tibet: Petrological and Geochemical Constraints. *Earth Science*, 34(1): 17－27 (in Chinese with English abstract).

Murphy, D. T., Collerson, K. D., Kamber, B. S., 2002. Lamproites from Gaussberg, Antarctica: Possible Transition Zone Melts of Archaean Subducted Sediments. *Journal of Petrology*, 43(6): 981－1001. https://doi.org/10.1093/petrology/43.6.981

Müller, D., Groves, D. I., 1993. Direct and Indirect Associations between Potassic Igneous Rocks, Shoshonites and Gold‐Copper Deposits. *Ore Geology Reviews*, 8(5): 383－406. https://doi.org/10.1016/0169-1368(93)90035-W

Palmer, M. R., Ersoy, E. Y., Akal, C., et al., 2019. A Short, Sharp Pulse of Potassium-Rich Volcanism during Continental Collision and Subduction. *Geology*, 47(11): 1079－1082. https://doi.org/10.1130/g45836.1

Pan, G. T., Wang, L. Q., Li, R. S., et al., 2012. Tectonic Evolution of the Qinghai‐Tibet Plateau. *Journal of Asian Earth Sciences*, 53: 3－14. https://doi. org/10.1016/j.jseaes.2011.12.018

Parendo, C. A., Jacobsen, S. B., Wang, K., 2017. K Isotopes as a Tracer of Seafloor Hydrothermal Alteration. *Proceedings of the National Academy of Sciences of the United States of America*, 114(8): 1827－1831. https://doi.org/10.1073/pnas.1609228114

Philpotts, J. A., Schnetzler, C. C., 1970. Phenocryst-Matrix Partition Coefficients for K, Rb, Sr and Ba, with Applications to Anorthosite and Basalt Genesis. *Geochimica et Cosmochimica Acta*, 34(3): 307－322. https://doi.org/10.1016/0016-7037(70)90108-0

Plank, T., 2014. The Chemical Composition of Subducting Sediments. Treatise on Geochemistry. Elsevier, Amsterdam, 607－629. https://doi.org/10.1016/b978-0-08-095975-7.00319-3

Prelević, D., Foley, S. F., Romer, R., et al., 2008. Mediterranean Tertiary Lamproites Derived from Multiple Source Components in Postcollisional Geodynamics. *Geochimica et Cosmochimica Acta*, 72(8): 2125－2156. https://doi.org/10.1016/j.gca.2008.01.029

Prelević, D., Jacob, D. E., Foley, S. F., 2013. Recycling Plus: A New Recipe for the Formation of Alpine‐Himalayan Orogenic Mantle Lithosphere. *Earth and Planetary Science Letters*, 362: 187－197. https://doi.org/10.1016/j.epsl.2012.11.035

Richter, F. M., Bruce Watson, E., Chaussidon, M., et al., 2014. Isotope Fractionation of Li and K in Silicate Liquids by Soret Diffusion. *Geochimica et Cosmochimica Acta*, 138: 136－145. https://doi. org/10.1016/j.gca.2014.04.012

Rudnick, R. L., Gao, S., 2014. Composition of the Continental Crust. Treatise on Geochemistry. Elsevier, Amsterdam, 1－51. https://doi.org/10.1016/b978-0-08-095975-7.00301-6

Santiago Ramos, D. P., Coogan, L. A., Murphy, J. G., et al., 2020. Low‐Temperature Oceanic Crust Alteration and the Isotopic Budgets of Potassium and Magnesium in Seawater. *Earth and Planetary Science Letters*, 541: 116290. https://doi.org/10.1016/j.epsl.2020.116290

Shen, Y., Zheng, Y. C., Hou, Z. Q., et al., 2021. Petrology of the Machangqing Complex in Southeastern Tibet: Implications for the Genesis of Potassium-Rich Adakite-Like Intrusions in Collisional Zones. *Journal of Petrology*, 62(11): egab066. https://doi. org/10.1093/petrology/egab066

Shen, Y., Zheng, Y. C., Hou, Z. Q., et al., 2022. Pre-Late Eocene Position of the Lüchun‐Jinping Microblock in Western Yangtze Craton: Constraints from Eocene‐Oligocene Lamprophyres in Southeastern Tibet. *Lithos*, 414: 106622. https://doi. org/10.1016/j.lithos.2022.106622

Soder, C. G., Romer, R. L., 2018. Post-Collisional Potassic-Ultrapotassic Magmatism of the Variscan Orogen: Implications for Mantle Metasomatism during Continental

Subduction. *Journal of Petrology*, 59(6): 1007－1034. https://doi.org/10.1093/petrology/egy053

Staudigel, H., Davies, G. R., Hart, S. R., et al., 1995. Large Scale Isotopic Sr, Nd and O Isotopic Anatomy of Altered Oceanic Crust: DSDP/ODP Sites 417/418. *Earth and Planetary Science Letters*, 130(1/2/3/4): 169－185. https://doi. org/10.1016/0012 - 821X(94)00263-X

Sun, S. S., McDonough, W. F., 1989. Chemical and Isotopic Systematics of Oceanic Basalts: Implications for Mantle Composition and Processes. *Geological Society, London, Special Publications*, 42(1): 313－345. https://doi.org/10.1144/GSL.SP.1989.042.01.19

Sun, Y., Teng, F. Z., Hu, Y., et al., 2020. Tracing Subducted Oceanic Slabs in the Mantle by Using Potassium Isotopes. *Geochimica et Cosmochimica Acta*, 278: 353－360. https://doi.org/10.1016/j.gca.2019.05.013

Sun, Y., Teng, F. Z., Pang, K. N., et al., 2021. Multistage Mantle Metasomatism Deciphered by Mg-Sr-Nd-Pb Isotopes in the Leucite Hills Lamproites. *Contributions to Mineralogy and Petrology*, 176(6): 45. https://doi.org/10.1007/s00410-021-01801-9

Teng, F. Z., Dauphas, N., Watkins, J. M., 2017. Non-Traditional Stable Isotopes: Retrospective and Prospective. *Reviews in Mineralogy and Geochemistry*, 82(1): 1－26. https://doi.org/10.2138/rmg.2017.82.1

Teng, F. Z., Hu, Y., Ma, J. L., et al., 2020. Potassium Isotope Fractionation during Continental Weathering and Implications for Global K Isotopic Balance. *Geochimica et Cosmochimica Acta*, 278: 261－271. https://doi.org/10.1016/j.gca.2020.02.029

Tian, S. H., Yang, Z. S., Hou, Z. Q., et al., 2017. Subduction of the Indian Lower Crust beneath Southern Tibet Revealed by the Post-Collisional Potassic and Ultrapotassic Rocks in SW Tibet. *Gondwana Research*, 41: 29－50. https://doi.org/10.1016/j.gr.2015.09.005

Tommasini, S., Avanzinelli, R., Conticelli, S., 2011. The Th/La and Sm/La Conundrum of the Tethyan Realm Lamproites. *Earth and Planetary Science Letters*, 301(3－4): 469－478. https://doi. org/10.1016/j.epsl.2010.11.023

Tuller-Ross, B., Marty, B., Chen, H., et al., 2019a. Potassium Isotope Systematics of Oceanic Basalts. *Geochimica et Cosmochimica Acta*, 259: 144－154. https://doi.org/10.1016/j.gca.2019.06.001

Tuller-Ross, B., Savage, P.S., Chen, H., et al., 2019b. Potassium Isotope Fractionation during Magmatic Differentiation of Basalt to Rhyolite. *Chemical Geology*, 525: 37－45. https://doi. org/10.1016/j. chemgeo.2019.07.017

Turner, S., Arnaud, N., Liu, J., et al., 1996. Post-Collision, Shoshonitic Volcanism on the Tibetan Plateau: Implications for Convective Thinning of the Lithosphere and the Source of Ocean Island Basalts. *Journal of Petrology*, 37(1): 45－71. https://doi. org/10.1093/petrology/37.1.45

Wang, J. H., Yin, A., Harrison, T. M., et al., 2001. A Tectonic Model for Cenozoic Igneous Activities in the Eastern Indo-Asian Collision Zone. *Earth and Planetary Science Letters*, 188(1/2): 123－133. https://doi. org/10.1016/S0012-821X(01)00315-6

Wang, K., Close, H. G., Tuller-Ross, B., et al., 2020. Global Average Potassium Isotope Composition of Modern Seawater. *ACS Earth and Space Chemistry*, 4(7): 1010－1017. https://pubs. acs. org/doi/abs/10.1021/acsearthspacechem.0c00047

Wang, K., Ionov, D. A., 2023. Potassium Isotope Evidence for Slab-Derived Fluids in the Sub-Arc Mantle. *Earth and Planetary Science Letters*, 619: 118315. https://doi.org/10.1016/j.epsl.2023.118315

Wang, K., Li, W. Q., Li, S. L., et al., 2021a. Geochemistry and Cosmochemistry of Potassium Stable Isotopes. *Geochemistry*, 81(3): 125786. https://doi.org/10.1016/j.chemer.2021.125786

Wang, Z. Z., Teng, F. Z., Prelević, D., et al., 2021b. Potassium Isotope Evidence for Sediment Recycling into the Orogenic Lithospheric Mantle. *Geochemical Perspectives Letters*, 18: 43－47. https://doi. org/10.7185/geochemlet.2123

Wang, Z. Z., Teng, F. Z., Busigny, V., et al., 2022a. Evidence from HP/UHP Metasediments for Recycling of Isotopically Heterogeneous Potassium into the Mantle. *American Mineralogist*, 107(3): 350－356. https://doi.org/10.2138/am-2021-7923

Wang, Z. Z., Teng, F. Z., Wu, F. Y., et al., 2022b. Extensive Crystal Fractionation of High-Silica Magmas Revealed by K Isotopes. *Science Advances*, 8(47): eabo4492. https://doi.org/10.1126/sciadv.abo4492

Workman, R. K., Hart, S. R., 2005. Major and Trace Element Composition of the Depleted MORB Mantle (DMM). *Earth and Planetary Science Letters*, 231(1/2): 53－72. https://doi.org/10.1016/j.epsl.2004.12.005

Xu, Y. G., Menzies, M. A., Thirlwall, M. F., et al., 2001. Exotic Lithosphere Mantle beneath the Western Yangtze Craton: Petrogenetic Links to Tibet Using Highly Magnesian Ultrapotassic Rocks. *Geology*, 29(9): 863.

https://doi. org/10.1130/0091 - 7613(2001)0290863:elmbtw>2.0.co;2

Yin, A., Harrison, T. M., 2000. Geologic Evolution of the Himalayan-Tibetan Orogen. *Annual Review of Earth and Planetary Sciences*, 28: 211－280. https://doi.org/10.1146/annurev.earth.28.1.211

Zeng, H., Rozsa, V. F., Nie, N. X., et al., 2019. Ab Initio Calculation of Equilibrium Isotopic Fractionations of Potassium and Rubidium in Minerals and Water. *ACS Earth and Space Chemistry*, 3(11): 2601－2612. https://doi.org/10.1021/acsearthspacechem.9b00180

Zhao, J. H., Li, Q. W., Liu, H., et al., 2018. Neoproterozoic Magmatism in the Western and Northern Margins of the Yangtze Block (South China) Controlled by Slab Subduction and Subduction - Transform - Edge - Propagator. *Earth - Science Reviews*, 187: 1－18. https://doi.org/10.1016/j.earscirev.2018.10.004

Zhao, Z. D., Mo, X. X., Dilek, Y., et al., 2009. Geochemical and Sr-Nd-Pb-O Isotopic Compositions of the Post-Collisional Ultrapotassic Magmatism in SW Tibet: Petrogenesis and Implications for India Intra-Continental Subduction beneath Southern Tibet. *Lithos*, 113(1－2): 190－212. https://doi.org/10.1016/j.lithos.2009.02.004

Zhu, Y., Lai, S. C., Qin, J. F., et al., 2021. Neoproterozoic Metasomatized Mantle beneath the Western Yangtze Block, South China: Evidence from Whole-Rock Geochemistry and Zircon U-Pb-Hf Isotopes of Mafic Rocks. *Journal of Asian Earth Sciences*, 206: 104616. https://doi.org/10.1016/j.jseaes.2020.104616

中文参考文献

莫宣学, 赵志丹, 朱弟成, 等, 2009. 西藏南部印度-亚洲碰撞带岩石圈: 岩石学-地球化学约束. 地球科学, 34(1): 17－27.